SCIENTIFIC JOURNAL OF MARITIME RESEARCH [POMORSTVO]
University of Rijeka FACULTY OF MARITIME STUDIES

https://doi.org/10.31217/p.39.2.1

A Long-Term Experimental Study on Evaluating Corrosion Currents in Reinforced Concrete for Marine Structures

Kazi Naimul Hoque[1*], Francisco Presuel-Moreno[2]

[1] Department of Naval Architecture and Marine Engineering, Bangladesh University of Engineering and Technology (BUET), BUET Central Road, Dhaka 1000, Bangladesh, e-mail: kazinaim@name.buet.ac.bd

[2] Department of Ocean and Mechanical Engineering, Florida Atlantic University (FAU), 101 North Beach Road, Dania Beach, FL 33004, USA, e-mail: fpresuel@fau.edu

* Corresponding author

ARTICLE INFO

Original scientific paper
Received 11 November 2024
Accepted 11 February 2025

Key words:
Concrete mix
Fly ash
Slag
Silica fume
Reservoir length
Electrochemical measurements
Corrosion current

ABSTRACT

This study investigates the corrosion currents in four reinforced concrete mixes—SL (cement replacement of 50% slag), FA (cement replacement of 20% fly ash), T1 (cement replacement of 50% slag and 20% fly ash), and T2 (cement replacement of 20% fly ash and 8% silica fume)—using an electromigration method to accelerate chloride transport and initiate corrosion within weeks/months. The corrosion propagation was monitored over 1600 days using electrochemical techniques such as Linear Polarization Resistance (LPR), Electrochemical Impedance Spectroscopy (EIS), and Galvanostatic Pulse (GP) measurements. The study evaluated how the composition of the concrete mixes and reservoir length influenced corrosion, by testing both binary mixes (SL and FA) and ternary mixes (T1 and T2). The results show that the LPR readings, which uses prolonged polarization, generally produces higher corrosion current values than GP readings, offering a dynamic view of corrosion but greater variability. The binary mixes with slag (SL) or fly ash (FA) exhibit higher corrosion currents, while ternary mixes, especially those containing fly ash and silica fume (T2), show reduced corrosion currents, suggesting improved resistance. The larger reservoir length contributed to higher corrosion currents, highlighting the critical influence of exposure conditions, concrete mix composition, and measurement techniques in evaluating corrosion. This underscores the importance of considering these factors collectively when assessing the durability and long-term performance of concrete in corrosive environments.

1 Introduction

The corrosion of steel reinforcement is a critical factor contributing to the degradation of reinforced concrete (RC) structures, significantly impacting their operational life and reliability. This phenomenon is especially relevant in marine environments, where structures like port docks, anchoring blocks, and offshore installations are exposed to aggressive environments that accelerate corrosion [1]. The performance and durability of these infrastructures are directly tied to their ability to resist such deterioration, as premature corrosion can lead to costly repairs or structural failure, jeopardizing safety and economic viability [2, 3].

Two primary mechanisms initiate the corrosion of steel in RC structures, chloride penetration and carbonation. Among these, chloride-induced corrosion is regarded as more severe due to its localized and aggressive nature. It often manifests as pitting corrosion, which can drastically reduce the cross-sectional area of the steel reinforcement, leading to significant structural implications [4]. In contrast, carbonation-induced corrosion progresses more uniformly and typically result in less severe damage under similar exposure conditions.

The progression of corrosion in RC structures is slow and influenced by multiple factors, including environmental exposure, material properties, and the quality of the concrete cover. This slow progression complicates data acquisition and delays critical maintenance or repair decisions. For instance, chloride penetration to critical levels under natural conditions can take anywhere from 10 to 50 years, depending on variables such as the con-

crete cover thickness and water-to-cementitious (w/cm) ratio [5–7]. Similarly, carbonation advances at a rate proportional to the square root of time, often requiring decades to cause substantial depassivation of the steel reinforcement [8–11].

Despite its critical implications, research on the long-term progression of natural corrosion remains limited due to the extensive timeframes required for observation [12–14]. This gap underscores the importance of accelerated testing methods and advanced modeling techniques to better understand and predict corrosion dynamics. It is crucial to address this challenge to develop more durable RC structures and improve maintenance strategies, especially for critical marine infrastructure.

To address these time constraints, accelerated corrosion testing has become a widely adopted experimental technique. These tests expedite the corrosion process by exposing specimens to artificially severe conditions, such as impressed current, elevated chloride concentrations, or controlled carbonation environments. This allows researchers to simulate various types of corrosion-induced damage, such as bond degradation between steel and concrete, cracking, spalling, and reductions in structural stiffness, within weeks or months instead of years [15–17]. For example, accelerated corrosion tests can induce visible cracking and measurable loss of reinforcement cross-section within a few hundred hours by applying currents of 100–1000 $\mu A/cm^2$, as opposed to the years required under natural exposure conditions [9].

Accelerated corrosion tests have proven invaluable in understanding the effects of corrosion on the mechanical and structural performance of RC elements. They provide insights into the timing of corrosion initiation and progression and enable researchers to study key parameters such as deformation capacity, ductility, bond strength, and failure mechanisms [18–20]. By simulating depassivation, cracking, and other processes, these tests facilitate observations of damage and structural deterioration within a compressed timeframe. This controlled and rapid experimentation provides critical data for designing maintenance strategies, assessing structural performance, and developing mitigation techniques for corrosion-related issues in RC structures [21].

In response to the need for more accurate modeling of corrosion propagation over an RC structure's lifespan, research is increasingly focused on developing methods that expedite corrosion initiation while still reflecting natural progression characteristics [22, 23]. This shift aims to enable reliable predictions of structural performance across various stages of corrosion, aiding in the design of more resilient RC structures and enhancing maintenance planning for existing infrastructure.

During the propagation stage of steel corrosion in concrete, accumulated corrosion products can reach critical volumes that lead to cracking and spalling. Studies commonly accelerate corrosion by introducing chlorides to concrete specimens and applying an electrical current, with high currents sometimes causing cracks within days to weeks [24-27]. Using a current density of 100 $\mu A/cm^2$ is seen as realistic for simulating field conditions, with experiments often sustaining this current for weeks to months [28-30]. Other research explores corrosion initiation and spread in pre-cracked concrete, with crack widths like 0.4 mm and 0.7 mm [31-33]. Sagüés and colleagues studied factors such as corrosion site length, rebar diameter, and concrete cover, finding that early corrosion may start as small pits (under 1 mm) in chloride-exposed areas, potentially protecting nearby steel, but coalescence of corrosion sites occurs over time [29, 30].

In the present study, four concrete mixes were tested. The anode length was controlled by adjusting the reservoir length, and chloride transport into the concrete was accelerated through electromigration, based on methods from previous studies [34]. Using this method, corrosion usually began within a few weeks to several months. The progression was monitored over around 1600 days through electrochemical impedance spectroscopy (EIS), linear polarization resistance (LPR), and galvanostatic pulse (GP) measurements, tracking changes in corrosion currents.

2 Materials and methods

2.1 Materials and mix proportions of concrete

In 2016, reinforced concrete samples were produced in two stages. The initial batch, containing binary mixes with either Fly Ash (FA) or Slag (SL), was prepared in April. A second batch, consisting of ternary mixes, fol-

Table 1 Concrete mix detail for SL, FA, T1 and T2 specimens

Mix	Cast Date	Cementitious Content	Cement Content	20% FA	8% SF	50% Slag	Fine agg.	Coarse agg.	w/cm ratio
		(kg/m^3)	(kg/m^3)	(kg/m^3)	(kg/m^3)	(kg/m^3)	(kg/m^3)	(kg/m^3)	
SL	4/4/2016	390	195	0	0	195	782	1009	0.41
FA	4/18/2016	390	312	78	0	0	967	833	0.41
T1	8/19/2016	390	117.5	78.3	0	195.2	761	1009	0.41
T2	8/19/2016	390	289	70	31	0	790	1046	0.37

lowed in August. Three mixes had a w/cm ratio of 0.41, while one was set at 0.37. Detailed compositions are outlined in Table 1, with further information available in reference [35].

The rebar had a radius of 0.47 cm, and was cut so that approximately 4 cm extended beyond the concrete. Prior to casting, these rebars were wire-brushed and cleaned with hexane to remove any grease. All these single rebar samples had dimensions of 30.5 cm x 12.7 cm x 7.6 cm. For each SL and FA mix, eleven single rebar specimens were prepared, each with a concrete cover of 0.75 cm. In contrast, five specimens (T1) and six specimens (T2) were created per mix, also with a 0.75 cm concrete cover. Each rebar was drilled, tapped, and fitted with a stainless-steel screw on one end to provide an electrical connection for corrosion monitoring.

During the casting process, all specimens were embedded with a stainless steel or titanium mixed metal oxide (TiMMO) mesh positioned on the top surface, which became the bottom surface during testing. This mesh served as an electrode to facilitate chloride ion transport. The reservoirs, designed to enhance localized chloride exposure, varied in length from 2.5 cm to 17.5 cm, with a consistent width of approximately 3 cm, and were centrally aligned along the rebar section. Specimen fabrication was conducted at the Florida Department of Transportation's State Materials Office (FDOT-SMO). After 24 hours, the molds were removed, and the specimens were moved to a fog room for curing, where they were stored for a minimum of 28 days to ensure proper hydration and strength development.

2.2 Specimen preparation for electromigration testing

Around late May 2016, SL and FA concrete samples were transported to FAU SeaTech campus for the next phase of experimentation, with T1 and T2 mixes following in mid-October. Upon arrival, all samples were stored in a high-humidity chamber to continue curing until the solution reservoirs were ready. Before installing the reservoirs for ponding, samples were transferred to a controlled lab environment (65% RH, and 21°C) for a few days.

Approximately 40 days post-casting, plastic reservoirs were mounted on the original top (molded) surface of each sample using marine-grade adhesive, with a 10% NaCl solution (by weight) added to each reservoir, centered along the rebar length to restrict corrosion initiation areas to the reservoir's length (ranging from 2.5 cm to 17.5 cm). The samples were humidified for 3–7 days, and meshes (stainless steel or TiMMO mesh) matching the embedded size were placed in the solution reservoirs. Each sample was then stored in a transparent plastic container, with about 1 cm of the base submerged in a saturated calcium hydroxide solution atop a white acrylic mesh to minimize leaching during electromigration.

2.3 Experimental setup and test procedure

A power supply was utilized to maintain a constant potential difference between the upper and lower mesh in each specimen, generating an electric field that facilitated the migration of chloride ions from the NaCl solu-

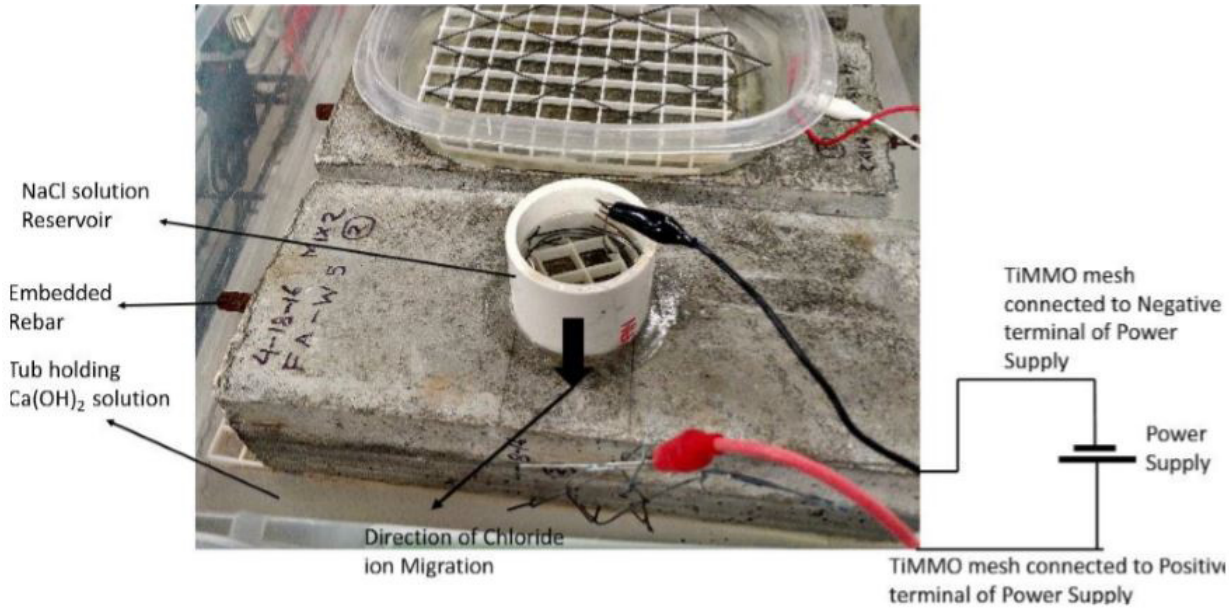

Figure 1 Experimental setup used for electromigration

tion reservoir into the concrete and toward the embedded rebar. The negative terminal of the power supply was connected to the electrode submerged in the NaCl solution reservoir, while the positive terminal was connected to the TiMMO mesh embedded within the concrete. To ensure that the TiMMO mesh did not directly contact the concrete surface, an acrylic mesh was placed in the solution reservoir, acting as a barrier while allowing ionic flow. Figure 1 provides a schematic representation of the electromigration setup, illustrating the key components and their arrangement.

Initially, the electromigration process was applied to all single-rebar specimens, including SL and FA mixes. The current flow was continuously monitored by measuring the potential drop across a 100-ohm resistor, allowing precise tracking of the current passing through the system during the controlled application of voltage over several days. At regular intervals, the power supply was disconnected to measure the rebar potential against a saturated calomel reference electrode (SCE). These measurements helped identify potential shifts that could signify the initiation of corrosion. If no signs of corrosion were detected, the rebar potential was monitored while disconnected, typically for at least two hours or longer, to observe potential stabilization. Once this assessment was complete, the electromigration process was resumed. This cycle of monitoring and restarting was repeated to ensure accurate tracking of chloride ingress and any related corrosion activity over the course of the experiment.

Different voltage levels were tested, starting with an initial potential of 9V; however, rebar potential measurements exceeded +2 V (SCE), a level that could induce pitting corrosion even at low chloride concentrations, prompting a reduction in the applied voltage to 3V [35]. The rebar potentials were monitored with the power on, immediately after disconnection, and at intervals of one and two hours as part of a depolarization test approach. These readings guided whether the system was reconnected to continue electromigration or left disconnected. At specified intervals, the system was turned off for two days or more to conduct LPR, EIS, and GP measurements, allowing natural chloride diffusion to continue during the pauses. In some cases, electromigration was stopped when the rebar potential failed to reach the corrosion initiation threshold of -0.200 V (SCE) or more negative, but monitoring persisted to observe chloride ingress and potential corrosion through diffusion [35].

3 Electrochemical measurements after corrosion initiation

Throughout the corrosion propagation stage, the rebar potential was regularly monitored using a SCE. At least two days post-disconnection, solution resistance (Rs) and corrected polarization resistance (Rc) were measured. Hence, Rc was determined by subtracting Rs from the apparent polarization resistance. LPR and EIS tests were conducted monthly on all specimens after initiation of corrosion by electromigration. EIS was conducted across a frequency range from 10 kHz to 1 Hz, identifying Rs at a frequency of 54.51 Hz, while LPR was measured from 10 mV below to 1 mV above the open circuit potential (OCP). Over time, LPR was adjusted to cathodic measurements starting from OCP, with scan rates set at either 0.1 mV/s or 0.05 mV/s. From January 2019, LPR and EIS readings decreased to bi-monthly or tri-monthly intervals, and from April 2019, these tests ceased.

In April/May 2017, GP testing commenced as an alternative method to determine Rs and Rc values. The GP test used a 10 μA pulse, maintaining polarization within 25 mV of the initial value. Measurements were extended to 300 seconds due to continued slope changes at 140 seconds, with subsequent tests conducted at 200 seconds as a balance. During GP tests, the rebar potential was measured initially at open circuit potential, followed by time-based measurements post-pulse to determine Rs and Rc values. The Rc values obtained from LPR/EIS and GP readings were converted to corrosion current (Icorr) values, as the exact corroding area was not known. The Icorr was calculated using the Stern-Geary equation: Icorr = B/Rp, where Rp (previously referred to as Rc) represents the polarization resistance, and B is the Stern-Geary constant, which varies between 13 and 52 mV depending on whether the steel is in a passive or active state of corrosion. For concrete, a common practice is to use 26 mV for actively corroding steel and 52 mV for passive steel, based on established research [36-38]. In this case, a value of 26 mV was selected.

4 Results and discussion

4.1 Evolution of Icorr with time obtained from LPR and GP measurements

The following section presents a comparative analysis of the evolution of Icorr values obtained from LPR and GP measurements for single rebar specimens cast with SL, FA, T1, and T2 over time. For SL and FA specimens, the Icorr plots are based on LPR measurements taken between June 2016 and May 2019, while GP measurements span from May 2017 to October 2020. Similarly, for T1 and T2 specimens, the Icorr plots are derived from LPR measurements recorded between November 2016 and May 2019 and GP measurements from May 2017 to October 2020. To facilitate meaningful comparisons, specimens with similar reservoir lengths are analyzed together.

Figure 2 illustrates the evolution of Icorr with time obtained from LPR and GP measurements for single rebar SL samples under 17.5 cm reservoir length. The LPR

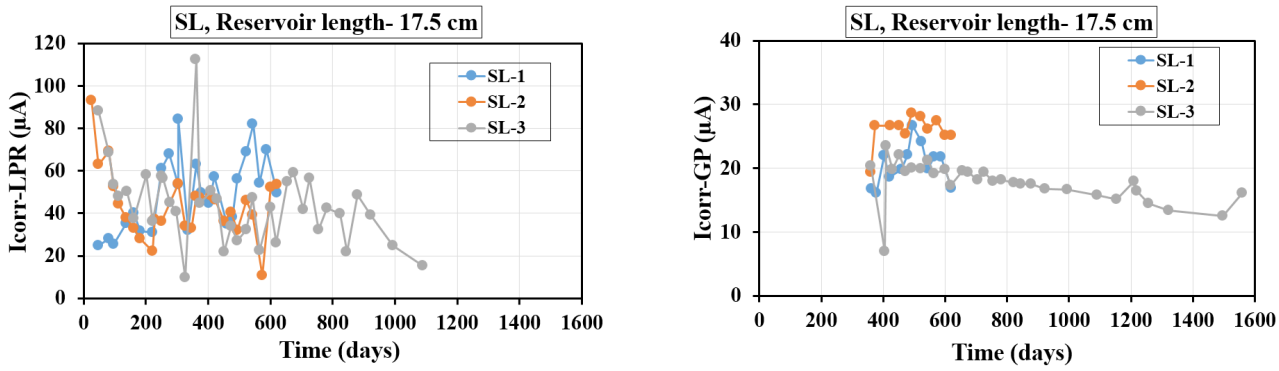

Figure 2 Icorr with time obtained from LPR and GP methods on selected single rebars (SL samples) under 17.5 cm reservoir length

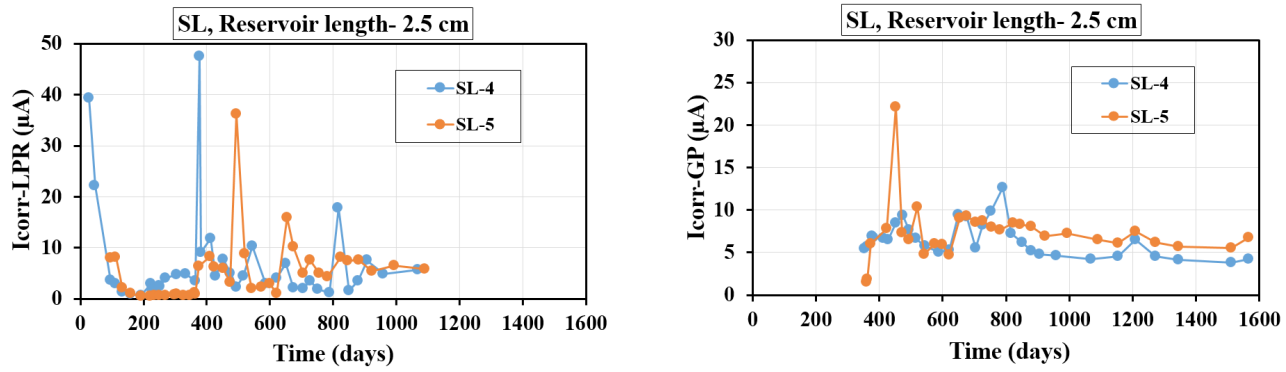

Figure 3 Icorr with time obtained from LPR and GP methods on selected single rebars (SL samples) under 2.5 cm reservoir length

measurements show significant fluctuations, especially during the initial phase (up to 600 days), with Icorr frequently exceeding 40 µA for certain samples like SL-1 and SL-2. In contrast, GP measurements exhibit a gradual rise in Icorr during the early phase, followed by stabilization at lower values. The LPR also shows greater variability across samples, likely due to its sensitivity to transient changes in corrosion dynamics, whereas GP provides more consistent and stable results with lower deviations. Over the long term, LPR measurements demonstrate a gradual decline in Icorr, although inconsistencies persist, while GP stabilizes more predictably, underscoring its reliability for long-term monitoring. Generally, LPR records higher Icorr values compared to GP, which tends to provide conservative readings that might underestimate transient peaks. Among the samples, SL-3 stands out with lower Icorr values in both methods, particularly in the long-term, possibly due to its unique characteristics like reduced permeability or better microstructure. The extended reservoir length of 17.5 cm appears to facilitate increased ionic transport, leading to higher Icorr values across both methods, with the effect being more pronounced in LPR data.

Figure 3 highlights the evolution of Icorr with time obtained from LPR and GP measurements for single rebar SL samples under 2.5 cm reservoir length. Both the plots indicate that the Icorr values generally decreased with time, stabilizing after approximately 600 days. However, some significant deviations are noted. The LPR plot shows sharper and more frequent spikes in Icorr values, particularly between 200 and 600 days, which might suggest a higher sensitivity to transient conditions or noise in the LPR measurements. Conversely, the GP measurements appear smoother and exhibit fewer pronounced spikes during the same period. Between the two samples (SL-4 and SL-5), the trends are broadly similar, but SL-5 tends to show slightly lower Icorr values after stabilization in both techniques, suggesting potentially better corrosion resistance. The results emphasize the importance of cross-comparing LPR and GP methods to ensure reliable corrosion monitoring over extended periods. The figures for the other SL samples can be found in these studies [39-41].

Figure 4 illustrates the evolution of Icorr with time for single rebar FA samples under 17.5 cm reservoir length, highlighting notable differences between LPR and GP measurements. The LPR plots for all samples (FA-7, FA-8, and FA-9) exhibit fluctuating trends, indicating periodic variations in corrosion activity over time. In contrast, the GP plots reveal more stable behav-

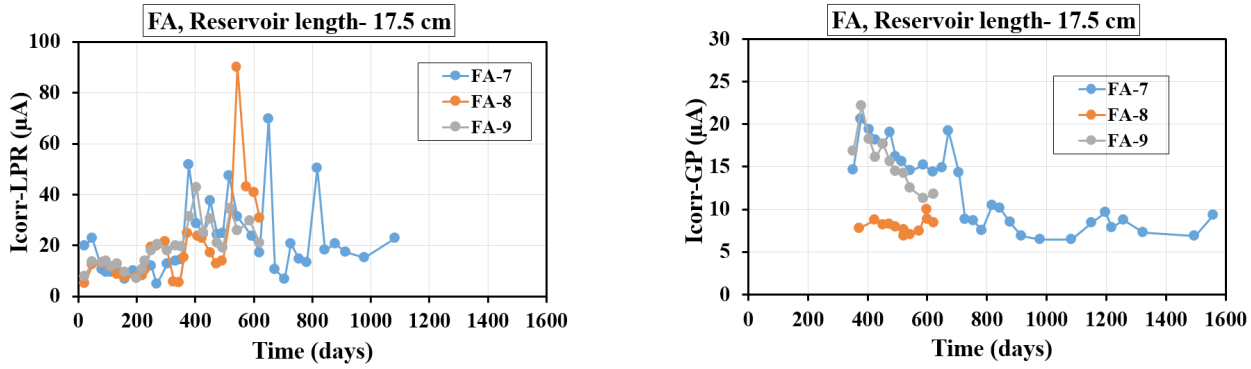

Figure 4 Icorr with time obtained from LPR and GP methods on selected single rebars (FA samples) under 17.5 cm reservoir length

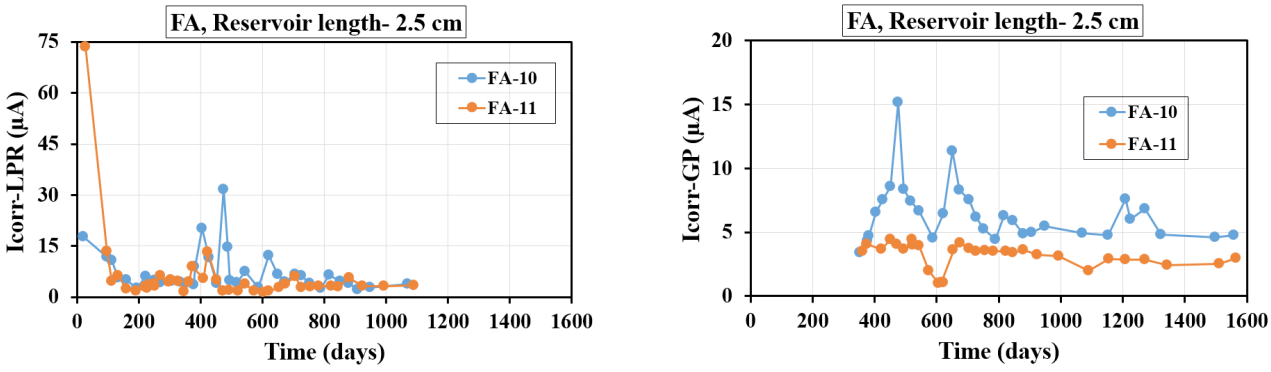

Figure 5 Icorr with time obtained from LPR and GP methods on selected single rebars (FA samples) under 2.5 cm reservoir length

iors, with FA-7 showing mild fluctuations, FA-8 maintaining a plateau trend, and FA-9 displaying a gradual decrease in Icorr starting from day 390. A key observation is that Icorr values measured by LPR are consistently higher than those obtained from GP, suggesting potential overestimation by LPR or differing sensitivities between the two techniques.

Figure 5 shows the evolution of Icorr with time for single rebar FA samples under 2.5 cm reservoir length, highlighting key differences between LPR and GP measurements. The LPR plots show distinct trends for the samples: FA-10 exhibits an initial decrease followed by a peak around day 480, while FA-11 displays a significant initial drop with subsequent fluctuations over time. In contrast, the GP plots for FA-10 show an increasing trend initially, reaching a peak at day 480, whereas FA-11 presents a stable plateau trend from 380–520 days, followed by a minimum around day 620 and a slight recovery leading to another plateau phase from 680–990 days. Notably, LPR measurements tend to show higher and more fluctuating Icorr values compared to the smoother trends observed in GP, emphasizing differences in sensitivity and transient behavior between the two techniques. These trends reflect the complex interaction of reservoir length and measurement methodology on corrosion dynamics. The figures for the other FA samples are available in studies [39-41].

Figure 6 illustrates the evolution of Icorr with time for single rebar T1 samples under 15 cm reservoir length, highlighting notable differences between LPR and GP measurements. The LPR plots show fluctuating trends for both samples, with T1-6 exhibiting consistent variations and T1-8 showing more pronounced fluctuations over time. In contrast, the GP plots reveal distinct trends: T1-6 reaches a peak around day 208 and stabilizes with slight fluctuations, while T1-8 initially increases until day 258, then decreases steadily until day 990, followed by minor fluctuations and a subsequent rise after day 1050. Notably, Icorr values obtained from LPR are consistently higher and more variable compared to the smoother trends observed in GP measurements. These results underscore the influence of reservoir length, cement composition, and measurement techniques on the observed corrosion behavior, with GP providing more stable and gradual trends relative to the fluctuating nature of LPR data.

Figure 7 illustrates the evolution of Icorr with time for single rebar T1 samples under 5 cm reservoir length, showcasing distinct behaviors between LPR and GP measurements. The LPR plots for both samples exhibit

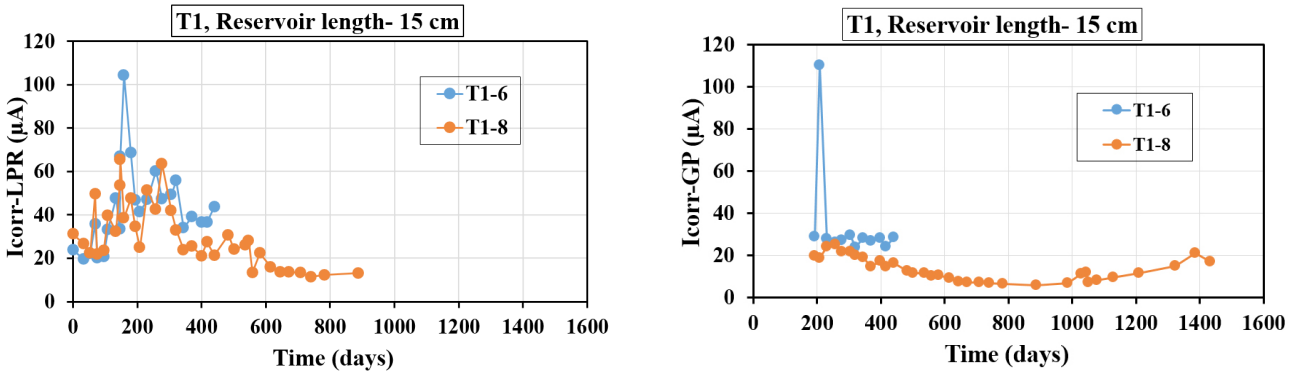

Figure 6 Icorr with time obtained from LPR and GP methods on selected single rebars (T1 samples) under 15 cm reservoir length

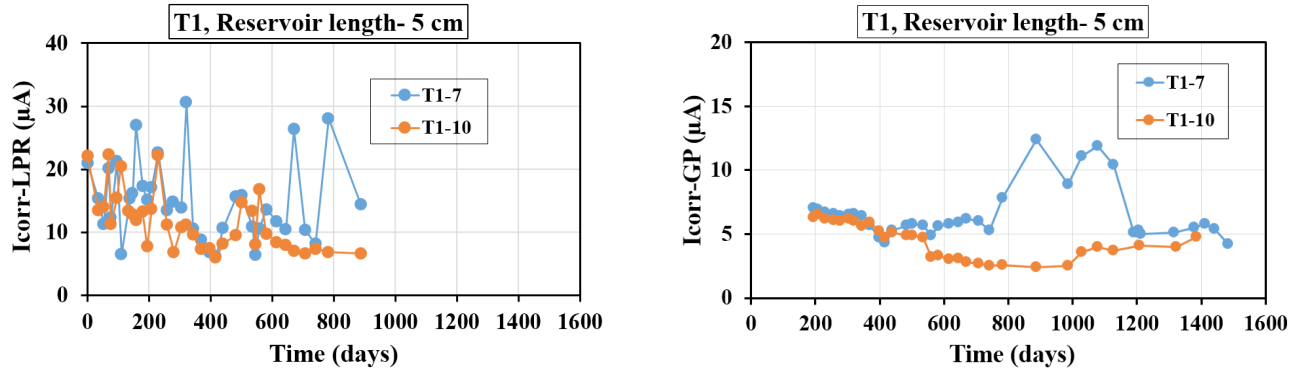

Figure 7 Icorr with time obtained from LPR and GP methods on selected single rebars (T1 samples) under 5 cm reservoir length

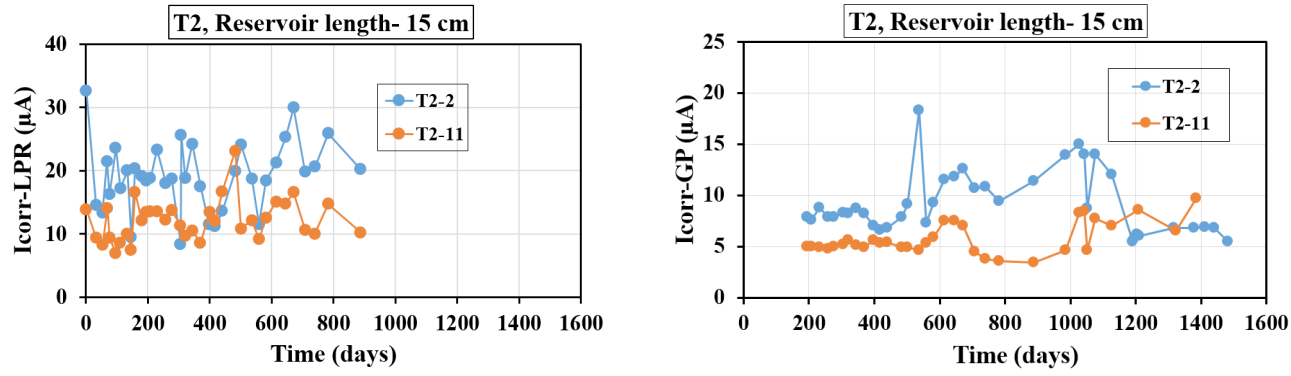

Figure 8 Icorr with time obtained from LPR and GP methods on selected single rebars (T2 samples) under 15 cm reservoir length

fluctuating trends, with T1-7 showing consistent variations and T1-10 reaching a peak around day 231 before continuing its fluctuations. In contrast, the GP plots reveal more stable and structured trends: T1-7 demonstrates a monotonic decrease until day 580, followed by an increase, and then a sharp decline after day 1177 when placed in a controlled environmental chamber. For T1-10, Icorr values decrease monotonically until day 590, followed by a plateau from 590–990 days, and then a gradual increase. A consistent observation is that Icorr values measured by LPR are significantly higher and more variable compared to those measured by GP, which show smoother and more predictable trends. The figures for the other T1 samples can be found in these studies [42-45].

Figure 8 depicts the evolution of Icorr with time for single rebar T2 samples under 15 cm reservoir length, highlighting differences between LPR and GP measurements. The LPR plots for T2-2 and T2-11 both exhibit fluctuating trends, with T2-11 reaching a peak around

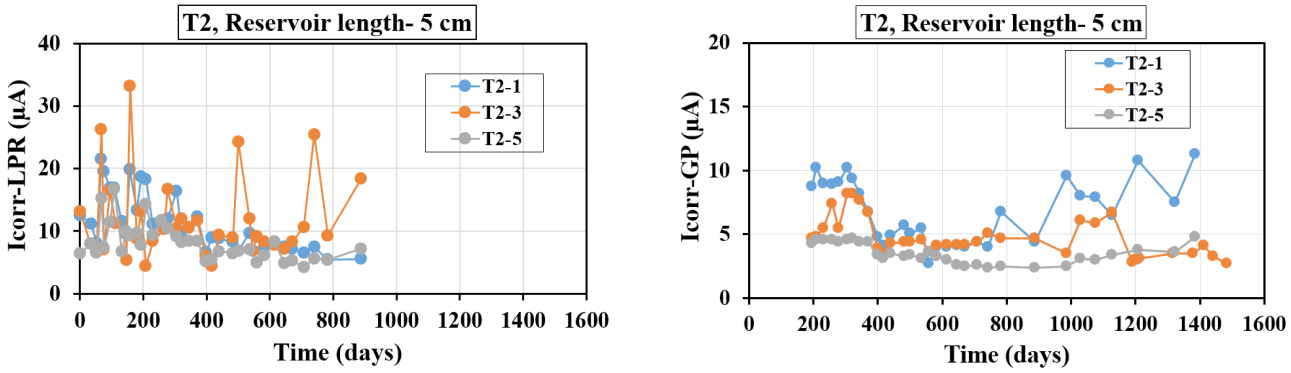

Figure 9 Icorr with time obtained from LPR and GP methods on selected single rebars (T2 samples) under 5 cm reservoir length

day 490. In contrast, GP measurements show more defined trends: T2-2 peaks at day 530, followed by fluctuations, and experiences a significant decrease after being transferred to a controlled environmental chamber on day 1177. The T2-11 initially follows a plateau trend until day 540, with minor fluctuations thereafter. A notable observation is that Icorr values from LPR are consistently higher and more variable than those from GP, which show smoother and more stable trends.

Figure 9 highlights the evolution of Icorr with time for single rebar T2 samples under 5 cm reservoir length, showcasing variations between LPR and GP measurements. The LPR plots for T2-1 and T2-5 show modest fluctuations over time, whereas T2-3 exhibits significant fluctuations, indicating a more variable corrosion process. In contrast, GP measurements reveal smoother trends, with T2-1 and T2-3 showing slight fluctuations, and T2-3 displaying a slight reduction in Icorr after being transferred to a controlled environmental chamber on day 1177. For T2-5, the GP plot initially demonstrates a plateau trend until day 370, followed by a monotonic decrease until day 890, and then a gradual increase thereafter. Notably, Icorr values obtained from LPR are consistently higher and more variable compared to the stable and gradual trends observed in GP measurements. These observations highlight the contrasting sensitivity and stability of the two methods in capturing corrosion activity under varying conditions. The figures for the other T2 samples can be found in studies [46-48].

The evolution of Icorr values for SL, FA, T1, and T2 specimens exhibit distinct trends over time, influenced by specimen type, reservoir length, and measurement techniques (LPR vs. GP). In general, LPR measurements tend to show higher and more fluctuating Icorr values, particularly during the early stages of exposure, suggesting greater sensitivity to transient corrosion activity. The SL and FA specimens, especially those with longer reservoir lengths, initially exhibit high Icorr values, followed by a gradual decline and eventual stabilization, with GP measurements displaying smoother trends compared to LPR measurements. The SL samples with shorter reservoir lengths tend to reach stabilization earlier, indicating reduced ionic transport and corrosion activity over time. The FA specimens show varied behavior, with some samples maintaining stable Icorr values while others experience intermittent peaks and declines. In contrast, T1 and T2 specimens follow similar patterns, with LPR data capturing significant fluctuations, while GP data provide a more stable depiction of corrosion evolution. Notably, T2 specimens, which typically show lower Icorr values, exhibit gradual reductions over time, reinforcing their enhanced corrosion resistance. The consistent disparity between LPR and GP measurements underscores the necessity of cross-referencing both techniques for reliable long-term corrosion assessment, as LPR captures transient peaks while GP provides a more conservative and stable representation of corrosion trends.

4.2 Icorr average and standard deviation (STD)

Figure 10 illustrates the Icorr average and STD values derived from LPR and GP measurements for single rebar samples of SL, FA, T1, and T2, categorized by reservoir length. The data for SL and FA samples were collected between July 2018 and April 2019 (10 sets of measurements), with the same timeframe applied to T1 and T2 samples. To maintain consistency in evaluating Icorr averages and STDs, the LPR and GP readings were aligned within the same timeframe, ensuring reliable comparisons across the different concrete mixes. A consistent trend of increasing Icorr values with longer reservoir lengths is evident across all mixes, underscoring the influence of chloride ingress facilitated by larger solution reservoirs. Among the mixes, SL samples showed the highest Icorr values, particularly in LPR measurements at the longest reservoir length (17.5 cm), reflecting their high susceptibility to corrosion in aggressive environments. For FA samples, though following a similar trend,

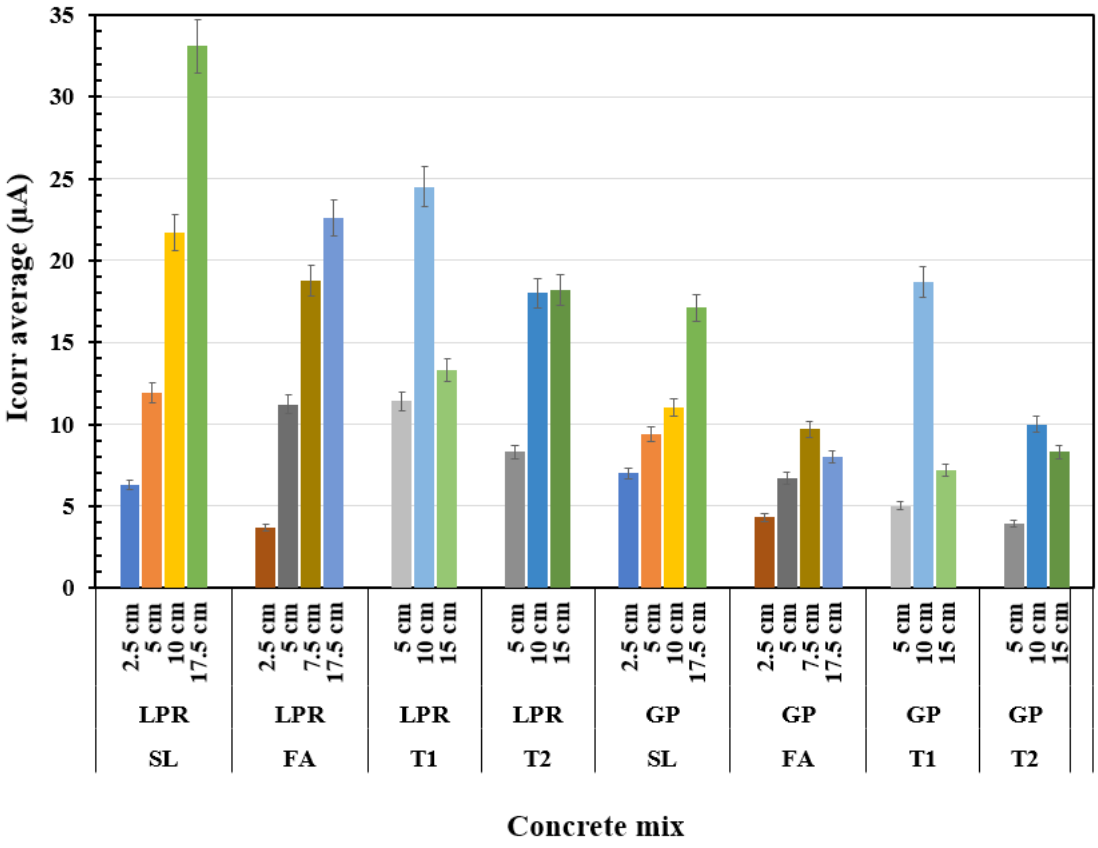

Figure 10 Variation in Icorr average from LPR and GP measurements based on reservoir length and concrete mixes cast with single rebar

exhibit lower Icorr values than SL samples, indicative of the improved resistance imparted by fly ash through its pore-refining pozzolanic effect. In case of T1 samples, combining slag and fly ash, display intermediate Icorr values, suggesting a balanced performance derived from the complementary properties of both supplementary cementitious materials (SCMs). In contrast, T2 samples, incorporating fly ash and silica fume, consistently demonstrate the lowest Icorr values, highlighting the superior corrosion resistance provided by silica fume's highly pozzolanic and densifying effects. A comparison of LPR and GP techniques reveals that LPR reports higher and more variable Icorr values, indicating its heightened sensitivity to localized corrosion processes, while GP provides lower, more stable readings, making it more reliable for assessing generalized corrosion. The performance of T1 and T2 mixes illustrates the effectiveness of combining multiple SCMs to enhance corrosion resistance, with T2 showing exceptional durability due to the inclusion of silica fume. The overall findings emphasize the critical roles of reservoir length, concrete mixes, and measurement technique in evaluating and improving the corrosion resistance of reinforced concrete exposed to chloride environments. The Icorr average values for SL samples have been documented in several studies, with reported values of 44.7 µA [7], 51.0 µA [49], and 13.8 µA [50], respectively. Similarly, for FA samples, the reported Icorr average values were 49.9 µA [7] and 17.6 µA [50], respectively. Furthermore, it has been observed that the Icorr values for T2 samples varied within the range of 9.7–25.3 µA, as reported in the literature [51].

The findings presented in Figure 10 underscores the superior corrosion resistance exhibited by ternary concrete mixes, particularly those incorporating silica fume (T2). The exceptional performance of T2 mixes can be attributed to silica fume's unique properties, including its high pozzolanic activity and ability to densify the cement matrix by refining the pore structure. This densification reduces the permeability of the concrete, limiting chloride ingress and the subsequent risk of rebar corrosion. Furthermore, the incorporation of fly ash in T2 mixes complements the benefits of silica fume by contributing additional pozzolanic reactions and enhancing long-term durability. The microstructural advantages provided by silica fume, such as the formation of a denser calcium silicate hydrate (C-S-H) gel and reduced capillary porosity, play a pivotal role in mitigating chloride diffusion. These improvements lead to a significant reduction in corrosion activity, as reflected in the consistently low Icorr values for T2 samples across all reservoir lengths.

In contrast, SL samples, which rely solely on slag as a supplementary cementitious material, exhibit the highest Icorr values, particularly under extended reservoir lengths. This suggests that while slag contributes to some durability improvements, it may not provide sufficient resistance to aggressive chloride environments when used alone. The intermediate performance of T1 mixes, combining slag and fly ash, highlights the partial mitigation of corrosion vulnerabilities through the synergistic effects of these two SCMs.

The consistent correlation between longer reservoir lengths and higher Icorr values across all mixes emphasizes the critical role of solution exposure in accelerating chloride-induced corrosion. Additionally, the comparison of electrochemical techniques (LPR and GP) reveals that LPR tends to overestimate corrosion currents due to its sensitivity to localized corrosion, whereas GP provides more reliable and stable measurements of generalized corrosion resistance.

These findings underscore the importance of leveraging advanced SCM combinations, particularly silica fume, to enhance the durability and service life of reinforced concrete in chloride-induced environments. A detailed microstructural analysis would further validate these observations by providing insights into pore structure, chloride binding capacity, and the distribution of hydration products.

5 General discussion

In examining the Icorr values for various concrete mixes over time, distinct patterns emerge between the measurement techniques, LPR and GP. Generally, LPR measurements yield higher Icorr values compared to GP measurements across most concrete samples. This discrepancy can be attributed to the methodological differences: LPR involves prolonged polarization of the rebar, potentially amplifying the measured corrosion activity, whereas GP uses a rapid pulse approach, resulting in more conservative and stable Icorr values. These variations highlight the importance of understanding the measurement techniques when interpreting corrosion behavior.

The study evaluates two primary types of concrete mixes: binary and ternary. The binary mixes consist of concrete incorporating either slag (SL) or fly ash (FA) as SCMs, while ternary mixes combine slag and fly ash (T1) or fly ash and silica fume (T2). The corrosion behavior differs significantly between these mixes, with binary mixes (SL and FA) generally displaying higher Icorr values than ternary mixes (T1 and T2). Among binary mixes, SL samples exhibit the highest Icorr values in both LPR and GP measurements, suggesting increased susceptibility to corrosion. This behavior may stem from the influence of slag on concrete permeability and its electrochemical characteristics, which can enhance ionic ingress under aggressive conditions. In contrast, FA samples tend to show lower Icorr values than SL, likely due to fly ash's pozzolanic effect, which refines the pore structure and reduces chloride penetration. The partial replacement of Portland cement with SCMs like slag and fly ash offers sustainability benefits to the construction industry, as noted by previous studies [52].

The ternary mixes (T1 and T2) demonstrate superior corrosion resistance, with lower Icorr values compared to binary mixes. This reduction is particularly pronounced in GP measurements. The enhanced performance of ternary mixes can be attributed to the synergistic effects of multiple SCMs, which densify the concrete matrix and reduce its permeability to corrosive ions. Notably, T2 samples consistently exhibit the lowest Icorr values among all mixes, indicating their exceptional durability. The inclusion of silica fume in T2 mixes likely contributes significantly to this performance, as silica fume enhances the concrete's microstructure by filling micro-pores and decreasing the connectivity of pore networks. This refinement reduces the ingress of aggressive agents, thereby improving the durability and corrosion resistance of the concrete.

The reservoir length also plays a critical role in influencing corrosion activity. The longer reservoir lengths (e.g., 15–17.5 cm) are generally associated with higher Icorr values across both binary and ternary mixes, as they facilitate greater ionic movement around the rebar. The SL samples with a 17.5 cm reservoir length display the highest Icorr values in both LPR and GP measurements, underscoring the impact of prolonged exposure conditions on corrosion rates. This trend suggests that the extent of solution exposure significantly accelerates corrosion processes, particularly in concrete mixes with higher permeability.

The measurement variability is another important consideration. The LPR measurements consistently show greater variability (higher standard deviation values) than GP measurements. This suggests that LPR captures more dynamic fluctuations in corrosion activity, possibly due to its sensitivity to localized corrosion processes. In contrast, GP measurements provide more stable and consistent results, with lower standard deviations, making them a reliable choice for applications requiring conservative and uniform corrosion assessments.

The study highlights several key insights into the corrosion behavior of reinforced concrete. The binary mixes, particularly SL, exhibit higher Icorr values compared to ternary mixes, emphasizing the role of SCM combinations in enhancing durability. The ternary mixes, especially T2, show the greatest reduction in corrosion activity, underscoring the effectiveness of combining fly ash and silica fume for improving concrete performance. The influence of reservoir length further underscores the importance of environmental exposure conditions, while the differences between LPR

and GP measurements emphasize the need to select appropriate techniques based on the specific requirements of durability assessments. These findings align with previous research [53, 54], which suggests that ternary mixes with silica fume provide superior resistance to corrosion, making them a preferred choice for reinforced concrete in chloride-laden environments.

6 Conclusion

The findings from this study provide valuable insights into the corrosion performance of concrete used in the maritime transportation industry and marine structures. The analysis of corrosion current values using LPR and GP methods highlights the influence of measurement techniques on monitoring outcomes. The LPR measurement, with its prolonged polarization, reveals dynamic fluctuations in corrosion activity, whereas GP measurement offers more stable and conservative readings, making it suitable for cautious monitoring strategies.

The study also underscores the critical role of SCMs in enhancing the durability of concrete mixes. The binary mixes, such as those with slag or fly ash, show higher corrosion currents, reflecting their greater susceptibility to aggressive environments. In contrast, ternary mixes, particularly those combining silica fume and fly ash (T2), demonstrate superior performance, with significantly lower corrosion currents. This improvement is attributed to the densification of the concrete matrix and reduced permeability, which effectively mitigate chloride-induced corrosion.

In addition, the effect of reservoir length on corrosion activity was observed, with larger reservoirs promoting higher corrosion currents due to increased ionic movement. This effect is most pronounced in slag-based binary mixes, while ternary mixes maintain better corrosion resistance even under these conditions.

Therefore, these findings highlight the importance of selecting appropriate concrete mix designs and monitoring techniques to improve the long-term durability and reliability of marine structures. The superior performance of ternary mixes, especially in aggressive environments, makes them a promising choice for enhancing the sustainability and safety of infrastructure in the maritime transportation industry.

Acknowledgement: The authors gratefully acknowledge the Florida Department of Transportation (FDOT) for their support in preparing the samples. The authors acknowledge the financial support provided by the FDOT (Grant No. BDV 27-977-08 FAU# AWD-000917) and the TriDurLE (Grant No. FAU# AWD-002175). The authors extend their gratitude to Florida Atlantic University and sincerely thank the graduate and undergraduate students from the Marine Materials and Corrosion Laboratory at FAU for their assistance with laboratory work and data collection. The opinions expressed in this paper are solely those of the authors and do not necessarily reflect the views of FAU, FDOT, or TriDurLE.

References

[1] Torres Martín JE, Ramos NR, Chinchón-Payá S, Arcila IH, Toledo AS, Montero JS, Sanjuán ML, Soto SA, García FO, Haan LD (2022) Durability of a reinforced concrete structure exposed to marine environment at the Málaga dock. Case Studies in Construction Materials, vol. 17, Article ID. e01582, pp. 1-17.

[2] Jones AEK (1997) Development of a holistic approach to ensure the durability of new concrete construction. British Cement Association, Crowthorne.

[3] Angst UM (2018) Challenges and opportunities in corrosion of steel in concrete. Mater. Struct., vol. 51(4), pp. 1–20.

[4] Broomfield JP (2007) Corrosion of steel in concrete-understanding, investigation and repair, 2nd edition. Taylor & Francis, Oxford.

[5] Castel A, Vidal T, Francois R, Arliguie G (2003) Influence of steel-concrete interface quality on reinforcement corrosion induced by chlorides. Mag. Concr. Res., vol. 55(2), pp. 151-160.

[6] Francois R, Arliguie G (1998) Influence of service cracking on reinforcement steel corrosion. J. Mater. Civ. Eng., vol. 10(1), pp. 14-20.

[7] Otieno M, Beushausen H, Alexander M (2016) Chloride-induced corrosion of steel in cracked concrete-part I: experimental studies under accelerated and natural marine environments. Cem. Concr. Res., vol. 79, pp. 373-385.

[8] Vidal T, Castel A, Francois R (2007) Corrosion process and structural performance of a 17-year-old reinforced concrete beam stored in chloride environment. Cem. Concr. Res., vol. 37(11), pp. 1551-1561.

[9] Zhang R, Castel A, Francois R (2009) Serviceability limit state criteria based on steel-concrete bond loss for corroded reinforced concrete in chloride environment. Mater. Struct., vol. 42(10), pp. 1407-1421.

[10] Zhang R, Castel A, Francois R (2009) The corrosion pattern of reinforcement and its influence on serviceability of reinforced concrete members in chloride environment. Cem. Concr. Res., vol. 39(11), pp. 1077-1086.

[11] Zhang R, Castel A, Francois R (2010) Concrete cover cracking with reinforcement corrosion of RC beam during chloride-induced corrosion process. Cem. Concr. Res., vol. 40(3), pp. 415-425.

[12] Ballim Y, Reid JC (2003) Reinforcement corrosion and the deflection of RC beams-an experimental critique of current test methods. Cement Concr. Compos., vol. 25(6), pp. 625-632.

[13] El Maaddawy T, Soudki K (2007) A model for prediction of time from corrosion initiation to corrosion cracking. Cement Concr. Compos., vol. 29(3), pp. 168-175.

[14] Liu Y, Weyers RE (1998) Modelling the time-to-corrosion cracking in chloride contaminated reinforced concrete structures. ACI Mater. J., vol. 95(6), pp. 675-681.

[15] Malumbela G, Moyo P, Alexander MG (2009) Behaviour of reinforced concrete beams under sustained service loads. Constr Build. Mater., vol. 23(11), pp. 3346-3351.

[16] Torres-Acosta AA, Fabela-Gallegos MJ, Munoz-Noval A, Vazques-Vega D, Hernandez-Jimenez JR (2004) Influence of corrosion on the structural stiffness of reinforced concrete beams. Corrosion, vol. 60(9), pp. 862-872.

[17] Torres-Acosta AA, Navarro-Guitierrez S, Teran-Guillen J (2007) Residual flexure capacity of corroded reinforced concrete beams. Eng. Struct., vol. 29(6), pp. 1145-1152.

[18] El Maaddawy T, Soudki KA (2003) Effectiveness of impressed current technique to simulate corrosion of steel reinforcement in concrete. ASCE J. Mater. Civ. Eng., vol. 15(1), pp. 41-47.

[19] Polder RB, Peelen HA (2002) Characterization of chloride transport and reinforcement corrosion in concrete under cyclic wetting and drying by electrical resistivity. Cem. Concr. Compos., vol. 24, pp. 427-435.

[20] Wu J, Li H, Wang Z, Liu J (2016) Transport model of chloride ions in concrete under loads and drying-wetting cycles. Constr. Build. Mater., vol. 112, pp. 733-738.

[21] Ye H, Jin X, Fu C, Jin N, Xu Y, Huang T (2016) Chloride penetration in concrete exposed to cyclic drying-wetting and carbonation. Constr. Build. Mater., vol. 112, pp. 457-463.

[22] Jung WY, Yoon YS, Sohn YM (2003) Predicting the remaining service life of land concrete by steel corrosion. Cem. Concr. Res., vol. 33(5), pp. 663-677.

[23] Otieno MB, Beushausen HD, Alexander MG (2016) Chloride-induced corrosion of steel in cracked concrete-part II: corrosion rate prediction models. Cem. Concr. Res., vol. 79, pp. 386-394.

[24] Andrade C, Alonso C, Molina FJ (1993) Cover Cracking as a Function of Rebar Corrosion: Part I -Experimental Test. Materials and Structures, vol. 26, pp. 453-464.

[25] Alonso C, Andrade C, Rodriguez J (1998) Factors Controlling Cracking of Concrete Affected by Reinforcement Corrosion. Materials and Structures, vol. 31, pp. 435 -441.

[26] Andrade C, Alonso C, Rodriguez J, Garcia M (1996) Cover Cracking and Amount of Rebar Corrosion: Importance of the Current Applied Accelerated Tests. Concrete Repair, Rehabilitation and Protection, R. K. Dhir and M. R. Jones, eds., E&FN Spon, London, pp. 263-273.

[27] Rasheeduzzafar, Al-Saadoun SS, Al-Gahtani AS (1992) Corrosion Cracking in Relation to Bar Diameter, Cover, and Concrete Quality. Journal of Materials in Civil Engineering, ASCE, vol. 4(4), pp. 327-342.

[28] Saeki N, Fujita Y, Takada N, Ohta T (1988) Control of Rust Damage of Reinforced Concrete in a Corrosive Environment. Concrete in Marine Environment, Proceedings of the Second International Conference, SP-109, V. M. Malhotra, ed., American Concrete Institute, Farmington Hills, Mich., pp. 163-177.

[29] Torres-Acosta A, Sagüés AA (2004) Concrete Cracking by Localized Steel Corrosion-Geometric Effects. ACI Materials Journal, vol. 101(6), pp. 501-507.

[30] Busba E, Sagüés AA (2013) Critical Localized Corrosion Penetration of Steel Reinforcement for Concrete Cover Cracking, CORROSION/2013, paper no. C2013-0002747 (Houston, TX).

[31] Otieno M, Beushausen H, Alexander M (2012) Prediction of corrosion rate in reinforced concrete structures-a critical review and preliminary results. Materials and Corrosion, vol. 63(9), pp. 777-790.

[32] Otieno MB, Alexander MG, Beushausen H (2010) Corrosion in cracked and uncracked concrete-influence of crack width, concrete quality and crack reopening. Magazine of Concrete Research, vol. 62(6), pp. 393-404.

[33] Vidal T, Castel A, Francois R (2004) Analyzing crack width to predict corrosion in reinforced concrete. Cement and Concrete Research, vol. 34, pp. 165-174.

[34] Presuel-Moreno F, Balasubramanian H, Wu Y (2013) Corrosion of reinforced concrete pipes: an accelerated approach. Corrosion 2013, paper no. C2013-0002551 (Houston, TX).

[35] Presuel-Moreno F, Nazim M, Tang F, Hoque K, Bencosme R (2018) Corrosion Propagation of Carbon Steel Rebars in High Performance Concrete. BDV27-977-08 Final Report for FDOT.

[36] Andrade C, Alonso C (1996) Corrosion rate monitoring in the laboratory and on-site. Constr. Build. Mater., vol. 10(5), pp. 315-328.

[37] Feliu V, Gonzalez JA, Feliu S (2007) Corrosion estimates from transient response to a potential step. Corros. Sci., vol. 49(8), pp. 3241-3255.

[38] Gonzalez JA, Miranda JM, Feliu S (2004) Consideration on the reproducibility of potential and corrosion rate measurements in reinforced concrete. Corros. Sci., vol. 46(10), pp. 2467-2485.

[39] Hoque K (2020) Corrosion propagation of reinforcing steel embedded in binary and ternary concrete. Ph.D. Dissertation, Department of Ocean and Mechanical Engineering, Florida Atlantic University (FAU), Boca Raton, Florida, USA.

[40] Presuel-Moreno F, Hoque K (2019) Corrosion propagation of carbon steel rebar embedded in concrete. Corrosion 2019, Nashville, Tennessee, USA.

[41] Hoque KN, Presuel-Moreno F (2023) Accelerated Corrosion of Steel Rebar in Concrete by Electromigration: Effect of Reservoir Length and Concrete Mixes. Proceedings of the 13th International Conference on Marine Technology (MARTEC 2022).

[42] Hoque KN, Presuel-Moreno F (2023) Corrosion Propagation of Steel Rebar Embedded in Marine Structures Prepared with Binary Blended Concrete Containing Slag. Proceedings of the 13th International Conference on Marine Technology (MARTEC 2022).

[43] Hoque KN, Presuel-Moreno F, Nazim M (2023) Corrosion of carbon steel rebar in binary blended concrete with accelerated chloride transport. Journal of Infrastructure Preservation and Resilience, vol. 4(26), pp. 1-15.

[44] Hoque KN, Presuel-Moreno F, Nazim M (2023) Accelerated Electromigration Approach to Evaluate Chloride-Induced Corrosion of Steel Rebar Embedded in Concrete. Advances in Materials Science and Engineering, Article ID. 6686519, pp. 1-14.

[45] Presuel-Moreno F, Hoque K, Rosa-Pagan A (2022) Corrosion propagation monitoring using galvanostatic pulse on reinforced concrete legacy samples. 2020-FAU-02 Final Report for National University Transportation Center TriDurLE.

[46] Hoque KN, Presuel-Moreno F (2023) Corrosion Behaviour of Reinforcing Steel Embedded in Fly Ash Concrete. Proceedings of the 13th International Conference on Marine Technology (MARTEC 2022).

[47] Hoque KN, Presuel-Moreno F (2023) Corrosion of Steel Rebar Embedded in Ternary Blended Concrete Exposed to High Humidity Environment. Proceedings of the 13th International Conference on Marine Technology (MARTEC 2022).

[48] Hoque KN, Presuel-Moreno F (2024) Electromigration-Based Investigation of Corrosion Behaviour in Ternary Blended Reinforced Concrete. International Journal of Structural and Civil Engineering Research, vol. 13(3), pp. 90-95.

[49] Hope BB, Ip AKC (1987) Corrosion of steel in concrete made with slag cement. ACI Materials Journal, vol. 84(6), pp. 525-531.

[50] O'Reilly M, Omid F, Darwin D (2019) Effect of Supplementary Cementitious Materials on Chloride Threshold and Corrosion Rate of Reinforcement. ACI Materials Journal, Title No. 116-M12, pp. 125-133.

[51] Kayali O, Zhu B (2005) Chloride induced reinforcement corrosion in lightweight aggregate high strength fly ash concrete. Construction and Building Materials, vol. 19, pp. 327-336.

[52] Johnson K, Garg A (2017) Partial Replacement of Wood Ash with Ordinary Portland Cement and Foundry Sand as Fine Aggregate. Journal of Civil and Environmental Engineering, vol. 7(2), Article ID. 1000272.

[53] Chao LC, Kuo CP (2017) Ternary Blends of High Aluminate Cement, Fly ash and Blast-furnace slag for Sewerage Lining Mortar. IOP Conference Series: Materials Science and Engineering, vol. 303(1), Article ID. 012023.

[54] Hoque KN, Presuel-Moreno F (2024) Chloride-induced corrosion of reinforcing steel embedded in ternary blended concrete. Journal of Naval Architecture and Marine Engineering, vol. 21(2), pp. 195–206.